Journal of Controlled Release 390 (2026) 114576

Contents lists available at ScienceDirect

Journal of Controlled Release

journal homepage: www.elsevier.com/locate/jconrel

Absorbable microspheres sustaining epirubicin and TLR7 agonist release for transarterial chemo-immuno-embolization in liver tumor

Yan Wang [a,1], Jiakun Guo [a,1], Di Hu [b], Hujing Tan [a], Wanting Chen [a], Chao Deng [a,*], Xiaoli Zhu [b,*], Zhiyuan Zhong [a,c,*]

[a] Biomedical Polymers Laboratory, and Jiangsu Key Laboratory of Advanced Functional Polymer Materials, College of Chemistry, Chemical Engineering and Materials Science, and State Key Laboratory of Radiation Medicine and Protection, Soochow University, Suzhou 215123, China
[b] Department of Interventional Radiology, The First Affiliated Hospital of Soochow University, Suzhou 215006, China
[c] College of Pharmaceutical Sciences, Soochow University, Suzhou, 215123, China

ARTICLE INFO

Keywords:
Biodegradable microspheres
Transarterial chemoembolization
Cancer immunotherapy
Controlled drug release
Hepatocellular carcinoma

ABSTRACT

Transarterial chemoembolization is a preferred medical intervention for unresectable advanced liver tumor patients. Its clinical efficacy is, nevertheless, undermined by poor control over drug release and immunosuppressed tumor microenvironment. In this work, we report on absorbable microspheres with excellent loading and controlled release of epirubicin and imiquimod, a toll-like receptor 7 agonist (EPI/IMQ@Asphere) for transarterial chemo-immuno-embolization (TACIE) in liver tumors. EPI/IMQ@Asphere while stable during storage steadily releases EPI in 4 weeks and IMQ in one week, continuously inducing immunogenic cell death and immune activation, respectively. Strikingly, one single injection of EPI/IMQ@Asphere into subcutaneous H22 murine liver tumor achieves complete regression in 5 out of 7 mice, all of which show complete resistance to tumor rechallenge, in line with robust and durable anti-cancer immune response. TACIE in orthotopic VX2 rabbit model reveals significant shrinkage of primary liver tumor and complete prevention of pulmonary metastasis, in which TACIE not only occludes tumor arteries and kills tumor cells but also amplifies tumoral $CD8^+/CD4^+$ T cell infiltration. Overall, TACIE based on EPI/IMQ@Asphere offers a highly appealing therapeutic strategy for advanced liver cancers.

1. Introduction

Hepatocellular carcinoma (HCC) stays as one of the most prevalent and high-mortality cancers globally [1,2]. A large body of HCC patients are diagnosed or will progress to advanced stages, in which tumors typically become unresectable and metastasis takes place [3]. Transarterial chemoembolization (TACE), which not only induces tumor arterial occlusion and cuts blood supply but also locally releases chemotherapeutics to the tumor site, is a preferred medical intervention for unresectable liver tumor patients [4–6]. Currently, several microspheres such as DC Bead®, HepaSphere®, and CalliSpheres® have entered the clinical practice to treat HCC, non-small cell lung cancer, renal cell carcinoma, etc. The therapeutic efficacy of existing TACE microspheres is, nevertheless, undermined by poor control over drug release, suboptimal embolization efficiency attributable to broad size distribution, and immunosuppressive tumor microenvironment, leading to progression and recurrence of residual tumors [7,8].

Cancer immunotherapy involving the activation of immune response against neoplasms has revolutionized clinical practices [9–14]. In advanced HCC management, monotherapy with immune checkpoint inhibitors (ICIs) typically confers objective response rates of 15–20 %. This therapeutic efficacy can be modestly promoted through strategic combinations with anti-angiogenic agents, dual ICI regimens, or tyrosine kinase inhibitors [15–19]. Recently, TACE has been shown to induce immune responses by induction of immunogenic cell death, stimulation of pro-inflammatory cytokine production, and reduction of exhausted effector cytotoxic T lymphocytes alongside regulatory T cell populations within tumor microenvironments [20–23]. Nevertheless, TACE monotherapy demonstrates inadequate capacity to sustain robust antitumor immunity against disease progression and relapse, strengthening the imperative for developing combinational immunotherapy alongside TACE [24,25].

* Corresponding authors.
E-mail addresses: cdeng@suda.edu.cn (C. Deng), zhuxiaoli90@163.com (X. Zhu), zyzhong@suda.edu.cn (Z. Zhong).
[1] **Yan Wang and Jiakun Guo contributed equally to this work**

https://doi.org/10.1016/j.jconrel.2025.114576
Received 25 August 2025; Received in revised form 14 December 2025; Accepted 22 December 2025
Available online 25 December 2025

Herein, absorbable microspheres with excellent loading and controlled release of epirubicin and imiquimod, a toll-like receptor 7 agonist (EPI/IMQ@Asphere) have been designed for transarterial chemo-immuno-embolization (TACIE) in advanced liver tumors (Scheme 1). Epirubicin (EPI) is selected as the chemotherapeutic agent due to its clinical prevalence in TACE for HCC, while additionally demonstrating induction capabilities of immunogenic cell death (ICD) to elicit antitumor immunity [26–28]. Imiquimod (IMQ), a potent Toll-like receptor 7 agonist with established clinical efficacy in condyloma acuminatum treatment, is strategically introduced to improve innate and adaptive immune responses through dendritic cell activation [29–31]. The formulation leverages hyaluronic acid-based microspheres that exploit strong electrostatic and hydrogen-bond interactions for efficient encapsulation and sustained release of both EPI and IMQ. In rabbits bearing orthotopic VX2 liver tumors, TACIE with EPI/IMQ@Asphere reveals significant shrinkage of primary liver tumor and complete prevention of pulmonary metastasis, in which TACIE not only occludes tumor arteries and kills tumor cells but also amplifies tumoral $CD8^+$/$CD4^+$ T cell infiltration. TACIE based on EPI/IMQ@Asphere establishes a robust platform for orchestrating TACE and immunotherapy, holding marvelous clinical potential for managing advanced liver tumors.

2. Experimental section

2.1. Preparation and characterization of EPI@Asphere and IMQ@Asphere

Asphere was prepared from hyaluronic acid-2-aminoethyl methacrylate derivative (HA-AMA, HA molecular weight: 9.0 kDa) via microfluidic and UV-initiated free radical polymerization (365 nm, 30 mW/cm^2) according to previous reports [19,32,44]. Briefly, the water phase was formulated by dissolving HA-*g*-MA (400 mg), I2959 (24 mg), and VA086 (4 mg) in 4 mL of PB (10 mM, pH 8.5), while the oil phage consisted of mineral oil containing 10 wt.% Span 80. Following filtration through a filter tip (450 nm), microdroplets were generated via hydrodynamic focusing in a microfluidic channel, and crosslinked under UV irradiation (365 nm, 30 mW/cm^2) for 20 min to obtain Asphere. Asphere was purified by sequential wash with isopropanol/n-hexane/PBS (2:3:1, *v/v/v*), isopropanol/PBS (1:1, v/v), and excessive PB. EPI@Asphere was obtained by direct mixing an Asphere suspension (25 mg/mL) with an equivalent volume of EPI solution to achieve theoretical DLC ranging from 10 wt.% to 20 wt.%. At predetermined time points, the unloaded EPI in the supernatant was quantified using a multifunctional microplate reader. The DLE and DLC were calculated according to the following formulations.

DLE (%) = Weight of drug loaded/Total weight of feed drug ×100.

DLC (wt.%) = Weight of drug loaded/Weight of drug and dried Asphere ×100.

IMQ@Asphere was prepared in a similar way, with additional stabilization achieved through the introduction of a tannic acid solution (2.0 mg/mL) following IMQ encapsulation. The unloaded IMQ in the supernatant was quantified using high-performance liquid chromatography (HPLC).

2.2. In vivo antitumor therapeutic efficacy and immunomodulation

H22 hepatoma murine model was established by subcutaneous injection of 2×10^7 H22 cells into the right hind leg of female Balb/c mice. When the tumor volume exceeded 100 mm^3, mice were randomly divided into 5 groups ($n = 7$) for one intratumoral administration with (1) PBS, (2) EPI/IMQ, (3) EPI@Asphere, (4) IMQ@Asphere, or (5) EPI/IMQ@Asphere (EPI: 5.0 mg/kg, IMQ: 2.5 mg/kg). Tumor volume and body weight were measured every 3 days. Tumor volume was calculated according to the formula $V=W^2 \times L/2$, where W and L represent lengths on the minor and long axes, respectively.

To explore the therapeutic mechanism of immunotherapy, tumor-bearing mice treated with different formulations for 10 d underwent systematic analysis. PBMCs were first isolated from blood collected via retro-orbital bleeding. Then, mice were sacrificed to extract tumors, spleens and tumor-draining lymph nodes (TDLNs). The tissues were processed into single-cell suspensions, blocked with CD16/32 antibodies, and stained with murine antibodies: PC5.5 CD45, FITC CD11b,

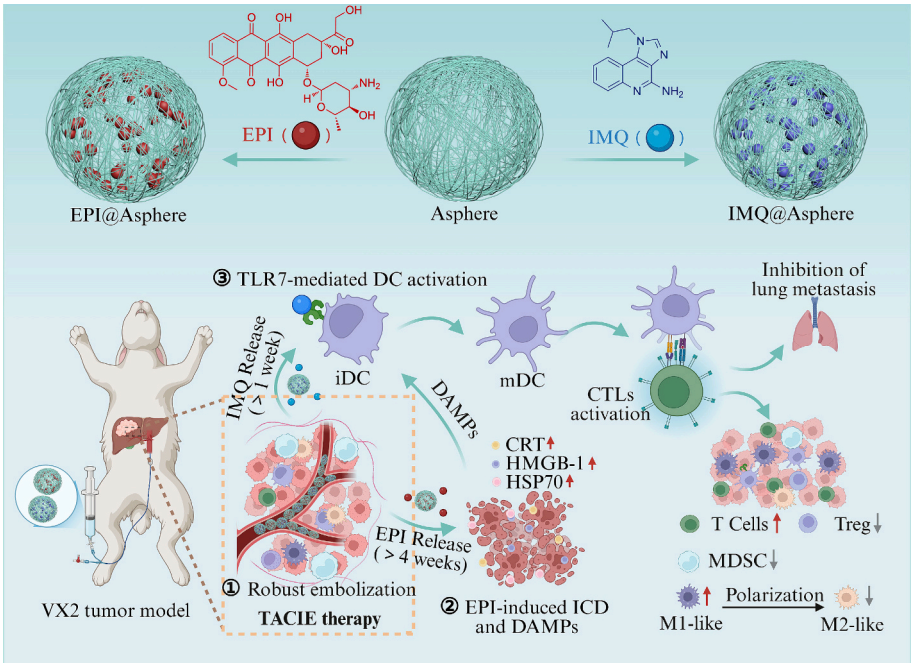

Scheme 1. Schematic illustration of absorbable microspheres with excellent loading and controlled release of epirubicin and imiquimod (EPI/IMQ@Asphere) for transarterial chemo-immuno-embolization (TACIE) in advanced liver tumors. In rabbits bearing orthotopic VX2 liver tumors, intraarterial administration of EPI/IMQ@Asphere demonstrated robust embolization of tumor arteries and significant infiltration of $CD8^+$/$CD4^+$ T lymphocytes within the tumors, leading to striking tumor regression and complete inhibition of tumor metastasis.

PE F4/80, AF647 CD206, PE-Cy7 CD86, FITC CD11c, PE MHC I, FITC CD3, PE CD4, PE-Cy7 CD8, PE-Cy7 CD25, AF647 Foxp3, and PE-Cy7 Gr1. Flow cytometry data were acquired on a flow cytometer (FACS Verse, BD Biosciences). and analyzed using FlowJo software. Immunohistochemical staining was used to analyze the infiltration of immune cells in distant tumors. Serum cytokines including interleukin-6 (IL-6), tumor necrosis factor-α (TNF-α), and interferon-γ (IFN-γ) were measured using an ELISA kit according to the manufacturer's protocol. Absorbance at 450 nm was measured using a microplate reader.

2.3. TACIE in orthotopic VX2 liver tumors

New Zealand white rabbits (2.5–3.0 kg) were used to establish an orthotopic VX2 liver tumor model. Briefly, rabbits were anesthetized and implanted with prepared VX2 tumor fragments (approximately 1.0 mm^3) into the left hepatic lobe. Tumor progression was monitored using CT and MRI imaging. When the tumor volume reaches approximately 800 mm^3, rabbits were randomly divided ($n = 3$), underwent transhepatic arterial catheterization, and administered with PBS, EPI@CalliSpheres (200 μL, EPI: 0.2 mg/kg), EPI@Asphere (200 μL, EPI: 0.2 mg/kg), and EPI/IMQ@Asphere (200 μL, EPI: 0.2 mg/kg, IMQ: 0.1 mg/kg) under the guidance with digital subtraction angiography (DSA). Tumor volume assessments were conducted weekly via CT imaging. Peripheral blood samples were obtained from auricular marginal veins on days 0, 3, 7, and 15. On day 14, rabbits were sacrificed for histopathological evaluation of tumors and major organs (heart, liver, spleen, lung, and kidney). Tumor necrosis was assessed through H&E staining, while $CD4^+$, $CD8^+$, $CD86^+$ and $Foxp3^+$ infiltration in tumors was analyzed via immunofluorescence staining. Tumor metastasis in the lung was quantified following paraformaldehyde fixation and histological processing. In addition, the blood samples (1.0 mL/rabbit) collected in procoagulant tubes underwent centrifugation (4 °C, 3000 rpm, 5 min) to isolate serum. Hepatic and renal function parameters including alanine aminotransferase (ALT), aspartate aminotransferase (AST), creatinine (Cr), and blood urea nitrogen (BUN) were measured via blood biochemical assays.

2.4. Statistical analysis

All results were presented as mean ± standard deviation (SD) and analyzed by using GraphPad Prism version 8.0. Multi-group comparisons were performed using one-way ANOVA. Statistical significance was set as follows: $^*p < 0.05$, $^{**}p < 0.01$, $^{***}p < 0.001$, $^{****}p < 0.0001$, and ns denoted no significant difference.

3. Results and discussion

3.1. Construction of therapeutic Asphere

Asphere with decent absorbability and biocompatibility was constructed from 2-aminoethyl methacrylate-functionalized hyaluronic acid using microfluidic and radical polymerization techniques as our previous report [32]. Asphere exhibited a highly uniform size of 90 μm with a coefficient of variation (CV) below 2 % and exceptional batch-to-batch reproducibility (Fig. S1). In contrast, most clinically used embolic spheres fabricated through conventional emulsion polymerization methods presented broader size distribution (CV > 20 %) and significant batch difference [32]. Notably, the scalable manufacturing of Asphere can be readily attained using multichannel microfluidic chip technology [33]. Under 20 U/mL HAase treatment, Asphere was progressively degraded, with the degradation mass of approximately 4 % in the first week and increasing to 23 % after 6 weeks (Fig. S2A). Moreover, obvious decrease of molecular weight was observed over time (Fig. S2B), further corroborating the decent degradability of Asphere.

Chemotherapeutics and immunoregulators were encapsulated into Asphere by direct blending of drugs with microsphere suspension, and additional tannic acid (TA) coating was applied for IMQ encapsulation. Notably, near-quantitative EPI loading in Asphere was achieved within 20 s even when the theoretical drug loading content (DLC) increased to 20 wt.% (Fig. 1A). Over 95 % drug loading efficiency (DLE) was obtained for EPI and IMQ when the theoretical DLC ranged from 10 to 20 wt.% (Fig. 1B-C). Both NaCl (disrupting electrostatic forces) and urea (interfering with hydrogen bonds) caused marked reductions in drug loading capacity (Fig. S3), highlighting the critical role of these intermolecular interactions in drug encapsulation. Notably, IMQ exhibited substantially higher sensitivity to NaCl and urea perturbations compared to EPI, which might be attributed to the fact that EPI was more prone to protonation and could provide abundant hydroxyl groups for multiple hydrogen bonds. The drug loading caused little influence on the size and morphology of Aspheres, with drug-loaded formulations (EPI@Asphere and IMQ@Asphere) maintaining uniform size distribution, spherical morphology, and smooth surfaces (Fig. 1D-E). In vitro release studies showed that sustained drug release from Asphere was attained in simulated tumor conditions (pH 6.5 + hyaluronidase (HAase)), in which EPI@Asphere exhibited prolonged release kinetics extending over 4 weeks (Fig. 1F). TA coating markedly modulated IMQ release behaviors, with increasing TA concentration to 2.0 mg/mL prolonging IMQ release to 1 week. Further increase of TA concentrations resulted in slight regulatory effect on drug release profiles while concurrently elevated microsphere viscosity (Fig. S4). Therefore, TA coating at 2.0 mg/mL was utilized for IMQ@Asphere formulation. Notably, EPI@Asphere and IMQ@Asphere following 90-d storage at 4 °C in PB at pH 7.4 exhibited little drug leakage (Fig. 1G), signifying their high stability. Compared to clinically used EPI@CalliSpheres, Asphere formulations displayed superior in vitro embolization in glass capillary tubes with less void fraction (**Fig. S5**).

3.2. In vitro antitumor effect and immunoactivation

The blank Asphere demonstrated favorable biocompatibility, maintaining over 95 % cell viability in L929 fibroblasts and H22 hepatoma cells after 24 h incubation at concentrations up to 1.0 mg/mL (Fig. 1H). As a commonly used chemotherapeutic agent in TACE treatment, EPI exerts cytotoxicity by directly intercalating with DNA base pairs and binding to DNA-associated enzymes [34,35]. Both EPI and EPI@Asphere showed dose-dependent cytotoxicity in H22 cells (Fig. 1I), confirming preserved antitumor efficacy post-microgel encapsulation. The comparable cytotoxicity between EPI@Asphere and free EPI was primarily attributed to the presence of NaCl in the cell culture media as well as extensive dilution (Fig. S6). Consistently, EPI@Asphere induced equivalent cell apoptosis to free drug, with over 20 % undergoing early-stage apoptosis and approximately 20 % progressing to late-stage apoptosis (Fig. 1J). The incorporation of immune microspheres (IMQ@Asphere) induced little influence on cytotoxicity and cell apoptosis.

Confocal laser scanning microscopy (CLSM) imaging revealed that H22 cells treated with EPI@Asphere for 24 h presented apparent surface exposure of calreticulin (CRT) and marked signal decrease of high mobility group box 1 (HMGB1) (Fig. 2A-B) owing to the translocation from the nucleus to cytoplasm, which are typically observed during immunogenic cell death (ICD) [36–38]. Quantitative analysis showed that EPI@Asphere caused approximately 4-fold upregulation of CRT expression, 3-fold elevation in HSP70 levels, 1.9-fold elevation of ATP release, and significant depletion of intracellular HMGB1 (Fig. 2C-E and Fig. S7). Compared to EPI@Asphere group, EPI/IMQ@Asphere revealed similar levels of CRT, HMGB1, ATP, and HSP70, signifying the little influence on ICD production of IMQ@Asphere. CRT exposure and HMGB1 translocation during ICD are known to drive the maturation of dendritic cells (DCs) [39,40]. IMQ as a TLR7 pathway agonist has been proved to assist antitumor immune responses through upregulation of co-stimulatory molecules, promotion of pro-inflammatory cytokine secretion, and augmentation of antigen presentation capacity [41]. Theimmunoactivation effects of EPI/IMQ@Asphere on bone marrow-

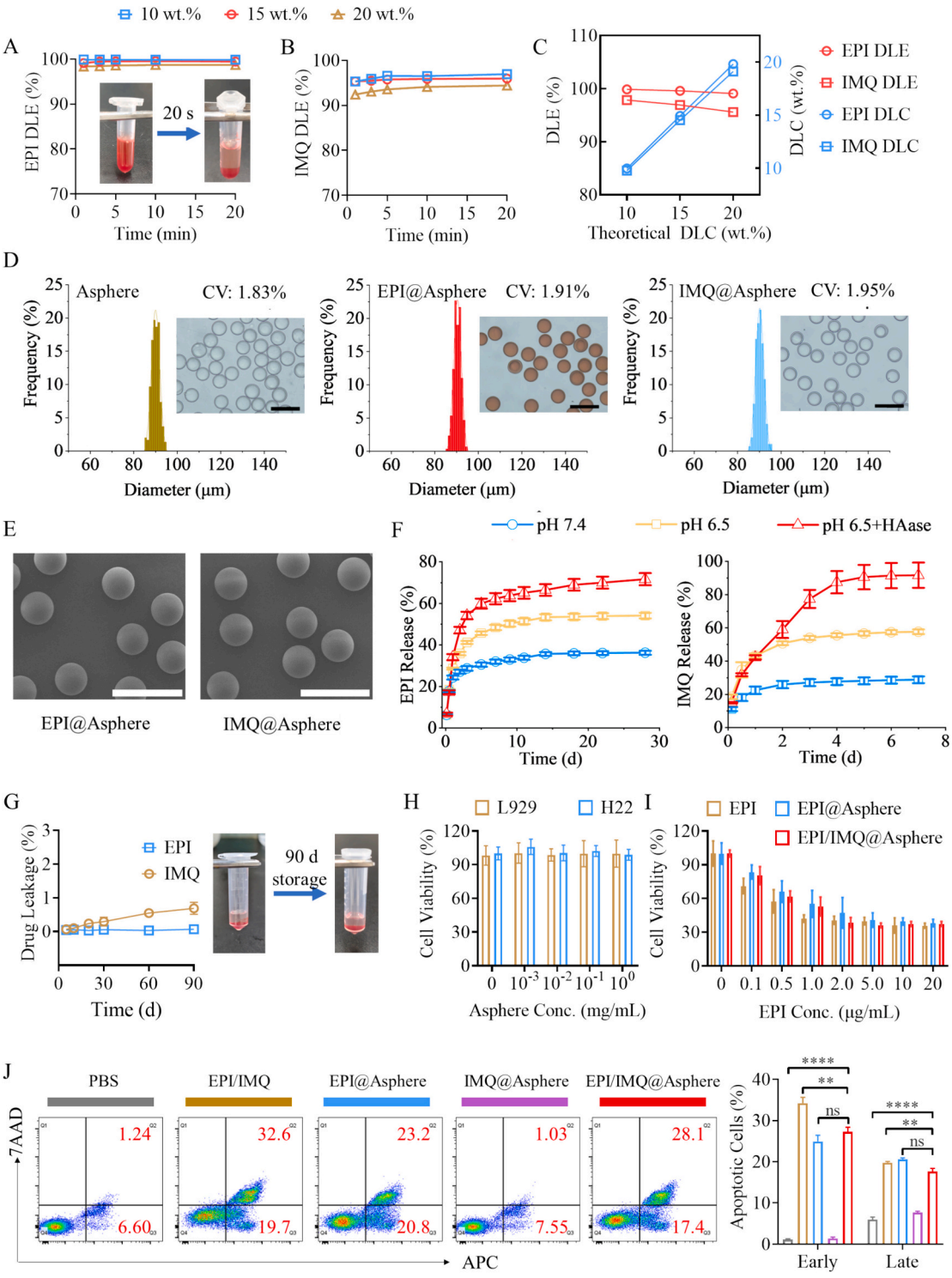

Fig. 1. Construction and characterization of chemoembolization microspheres loaded with epirubicin (EPI@Asphere) and immune microspheres loaded with imiquimod (IMQ@Asphere), $n = 3$. (A) EPI loading in Asphere over time. (B) IMQ loading in Asphere over time. (C) Drug loading efficiency (DLE) and drug loading content (DLC) of EPI and IMQ in Asphere. (D) Size distribution and microscope images of Asphere, EPI@Asphere, and IMQ@Asphere. Scale bars, 200 μm. (E) Scanning electron microscopy (SEM) images of EPI@Asphere and IMQ@Asphere. Scale bars, 100 μm. (F) In vitro release curves of EPI and IMQ from Asphere at pH 7.4, pH 6.5, and pH 6.5 + hyaluronidase (HAase). (G) Storage stability of EPI@Asphere and IMQ@Asphere in PB at pH 7.4. (H) Cytocompatibility of Asphere toward L929 and H22 cells after 24 h incubation. (I) Cytotoxicity of EPI@Asphere toward H22 cells after 24 h incubation. (J) Representative flow cytometry graphs and quantitative apoptosis analysis in H22 cells. Data are presented as the mean ± SD. Statistical significance was analyzed by one-way ANOVA using Tukey's posttest. *p* value: $^{*}p < 0.05$, $^{**}p < 0.01$, $^{***}p < 0.001$, $^{****}p < 0.0001$.

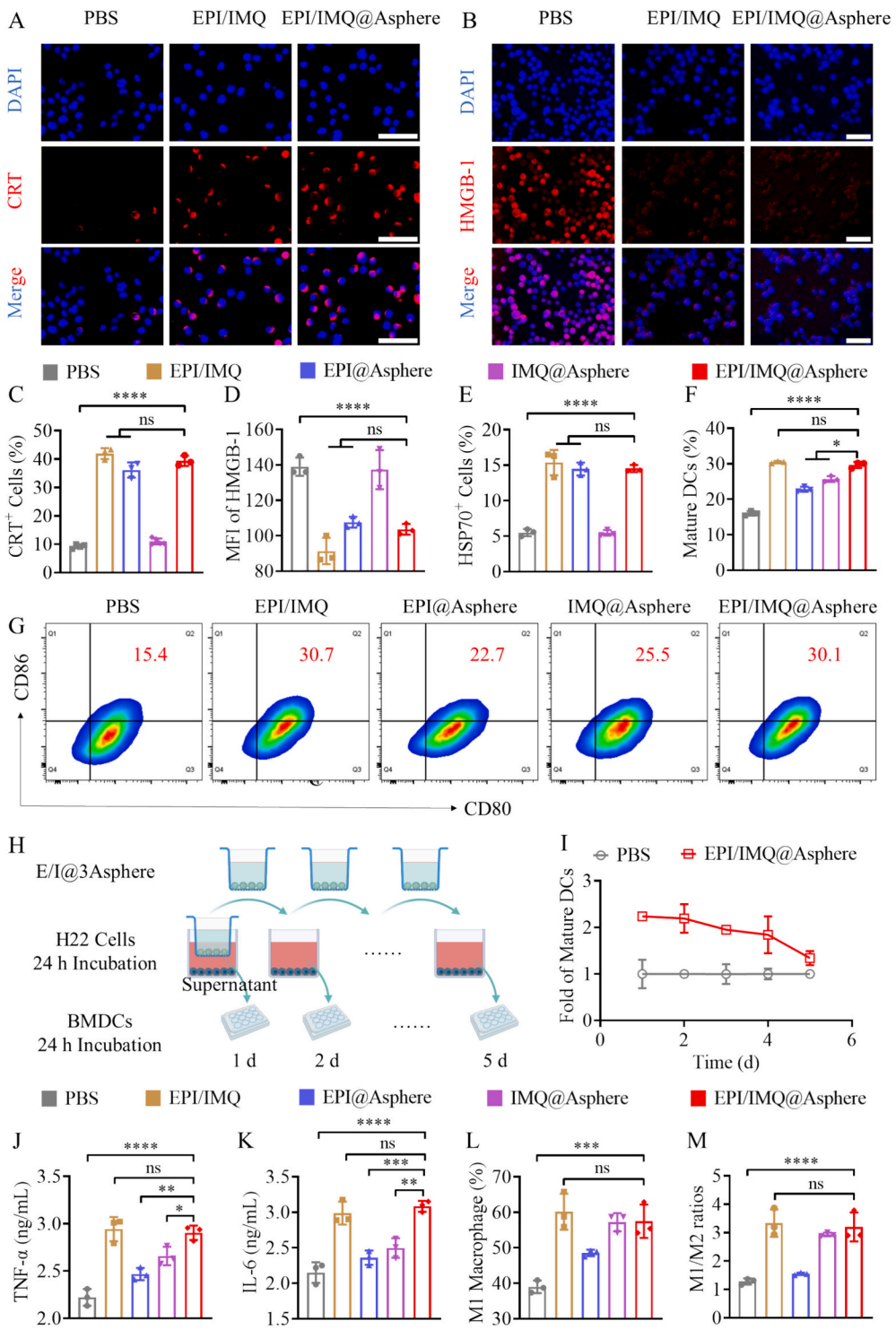

Fig. 2. Immunogenic cell death (ICD) and immunoactivation effects on bone marrow-derived dendritic cells (BMDCs) and macrophages (BMDMs), $n = 3$. (A-B) CLSM images of H22 cells stained with APC-labeled CRT (A) and HMGB1 (B) antibodies. The cells were incubated with different formulations for 24 h. Scale bars, 50 μm. (C-E) Flow cytometry analysis of CRT (C), HMGB-1 (D), and HSP70 (E) expression in H22 cells. The cells were treated with different formulations for 24 h, and then the supernatant was added into BMDCs or BMDMs for another 24 h incubation. (F) Quantification analysis of the mature DCs ($CD80^+CD86^+$). (G) Representative flow cytometry graphs of $CD80^+CD86^+$ cells in BMDCs. (H) Schematic diagram of sustained DC activation. (I) Quantification of $CD80^+CD86^+$ cells in BMDCs. H22 cells were treated with EPI/IMQ@Asphere for 24 h on days 1 through 5, and then the supernatant was added into BMDCs for another 24 h incubation. The results are expressed as the fold change relative to the corresponding level in PBS group. (J-K) Cytokine secretion of TNF-α (J) and IL-6 (K) in BMDCs. (L) Quantification analysis of M1 macrophages. (M) Quantification analysis of M1/M2 ratios. Data are presented as the mean ± SD. Statistical significance was analyzed by one-way ANOVA using Tukey's posttest. p value: $^*p < 0.05$, $^{**}p < 0.01$, $^{***}p < 0.001$, $^{****}p < 0.0001$.

derived dendritic cells. (BMDCs) and macrophages (BMDMs) were further investigated by treating the cells with the supernatant from H22 cells incubated with different formulations for 24 h. Notably, EPI@Asphere, IMQ@Asphere, and EPI/IMQ@Asphere all induced significant increase of $CD80^+CD86^+$ BMDCs, in which EPI/IMQ@Asphere demonstrated the highest and persistent BMDC activation for 5 days (Fig. 2F-I). Compared to PBS group, all treatment groups revealed higher secretion levels of immunostimulatory factors including interleukin-6 (IL-6) and tumor necrosis factor-α (TNF-α) (Fig. 2J-K), corroborating the dual regulatory mechanism in amplifying antitumor immunity through coordinated ICD signaling and TLR pathway activation by EPI/IMQ@Asphere. Notably, EPI/IMQ, IMQ@Asphere, and EPI/IMQ@Asphere markedly elevate M1 macrophage subsets and the M1/M2 ratio (Fig. 2L-M and Fig. S8), signifying their capacity to polarize macrophage toward a pro-inflammatory phenotype.

3.3. *In vivo antitumor efficacy and immune regulation of EPI/IMQ@Asphere*

In vivo pharmacokinetic studies in subcutaneous H22 hepatoma-bearing mice revealed that EPI/IMQ@Asphere group exhibited drug concentrations below 100 ng/mL in the plasma throughout the whole experimental period, suggesting minimal systemic drug exposure and related adverse toxicity. In contrast, the administration of free EPI/IMQ led to rapid systemic absorption, achieving peak plasma concentrations of 170 ng/mL EPI and 130 ng/mL IMQ within 30 min post-injection, which were over 2-fold higher than those in EPI/IMQ@Asphere group (Fig. S9). In vivo biodistribution studies revealed that mice treated with EPI/IMQ@Asphere showed minimal drug deposition in vital organs over 24 h, while free drug injection caused discernable EPI accumulation in healthy organs including the kidney, lung, and spleen particularly 1 h post-administration (Fig. S10). Notably, EPI/IMQ@Asphere group

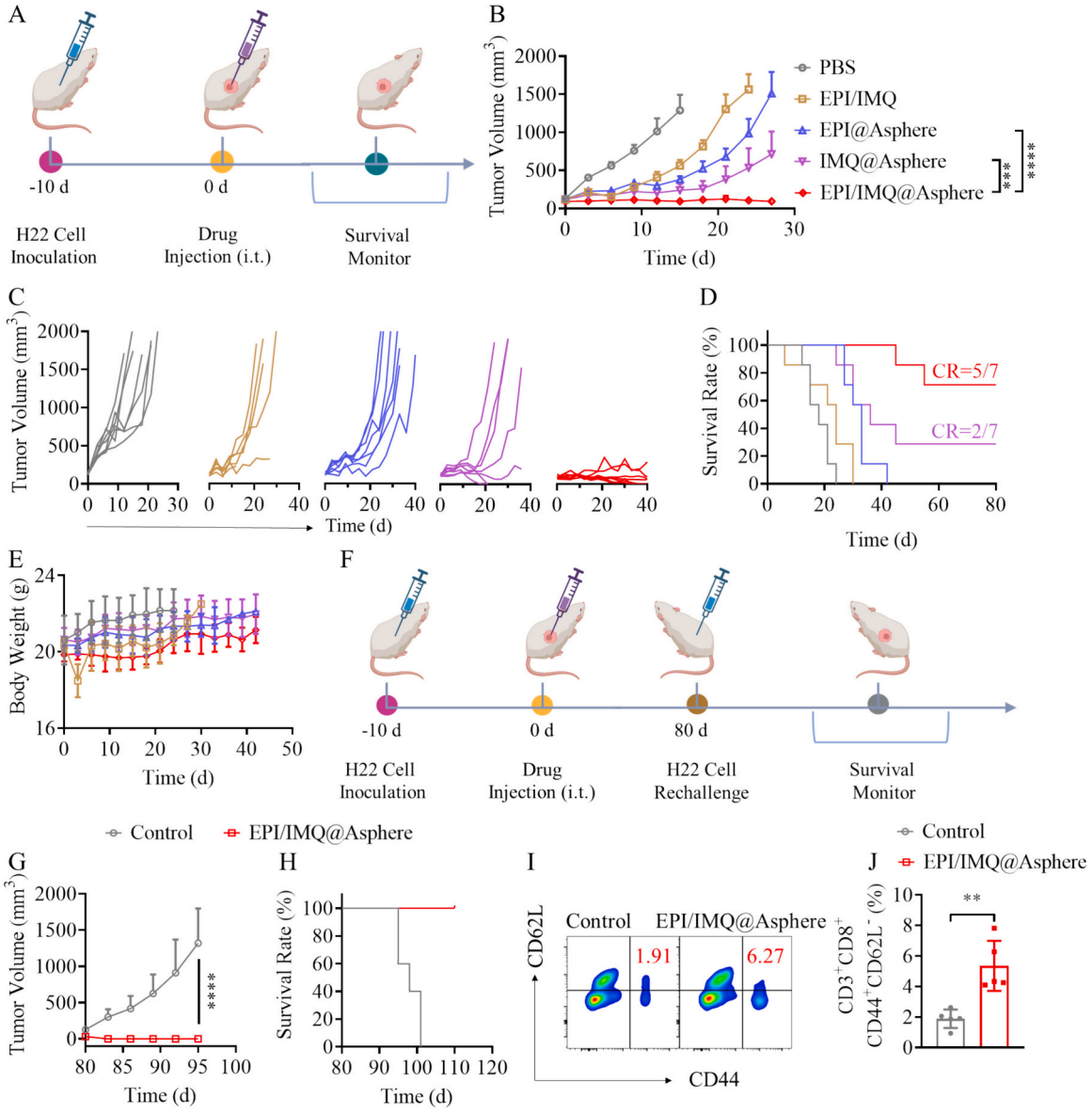

Fig. 3. Antitumor efficacy and tumor rechallenge in subcutaneous H22 tumor model. (A) Schematic diagram of the treatment of H22 tumor model, $n = 7$. (B) Average tumor growth curves. (C) Individual tumor growth curves. (D) Survival curves. (E) Body weight. (F) Schematic diagram of rechallenge and immunomemory analysis of H22 tumor model, $n = 5$. (G) Tumor growth curves following the rechallenge with H22 cells. (H) Survival curves. (I) Representative flow cytometry graphs of T_{EM} cells ($CD44^+CD62L^-$) among $CD3^+CD8^+$ T cells in peripheral blood (PB) on day 20 post-rechallenge. (J) Quantitative analysis of T_{EM} cells in $CD3^+CD8^+$ T cells in PB. Data are presented as the mean ± SD. Statistical significance was analyzed by one-way ANOVA using Tukey's posttest. p value: $^*p < 0.05$, $^{**}p < 0.01$, $^{***}p < 0.001$, $^{****}p < 0.0001$.

demonstrated much higher drug enrichment in tumor tissues than the free EPI/IMQ formulation, indicating enhanced and sustained therapeutic efficacy.

The in vivo antitumor efficacy of drug-loaded microspheres was systematically evaluated using subcutaneous H22 hepatoma-bearing mice (Fig. 3A). A single intratumoral administration of EPI/IMQ@Asphere at an EPI dose of 5.0 mg/kg revealed that increasing IMQ from 1.25 mg/kg to 2.5 mg/kg markedly improved tumor suppression, while further elevating IMQ yielded no additional benefit (Fig. S11). Conversely, when IMQ was fixed at 2.5 mg/kg, raising EPI from 2.5 mg/kg to 5.0 mg/kg significantly enhanced therapeutic efficacy. Thus, 5.0 mg/kg EPI, 2.5 mg/kg IMQ, and EPI/IMQ ratio of 2 were utilized in subsequent in vivo evaluation. Intratumoral injection of free drugs served as the control group to ensure tumor drug concentrations equivalent to those achieved with Asphere formulations, enabling an accurate assessment of the therapeutic advantages conferred by Asphere delivery systems. EPI@Asphere and IMQ@Asphere were administered at the same total microsphere dosage as the combination group to eliminate the potential influence on embolization efficacy due to variations in microsphere quantity. In sharp contrast to swift tumor growth in PBS and free EPI/IMQ groups, one single intratumoral injection of EPI@Asphere, IMQ@Asphere, or EPI/IMQ@Asphere elicited significant tumor growth suppression (Fig. 3B-D), signifying the critical role of sustained drug release from the microspheres. Strikingly, EPI/IMQ@Asphere induced complete tumor regression in 5/7 mice within 80 day observation, demonstrating robust and durable antitumor immunity. Besides, the combination of EPI@Asphere + free IMQ although efficiently suppressed the tumor progression, it failed to induce complete remission in any treated mice and merely extended the median survival by 36 days (Fig. S12), highlighting the necessity of sustained release of both drugs to realize the synergistic potential. Importantly, no obvious body weight reduction was observed in microparticle-based formulation throughout the study period, whereas mice receiving free EPI/IMQ combination showed progressive weight decline (Fig. 3E). Thus, EPI/IMQ@Asphere with significantly therapeutic efficacy and favorable safety profile holds great potential for combination immunotherapy.

Encouraged by the exceptional antitumor performance of EPI/IMQ@Asphere, we further assessed the immune memory establishment by re-attacking cured mice with H22 tumor cells on day 80 post-treatment (Fig. 3F). Healthy mice inoculated with tumor cells served as a control group. Strikingly, cured mice exhibited complete abrogation of tumor progression accompanied by 100 % survival rates, in contrast with the aggressive tumor growth observed in the control group (Fig. 3G-H). Effector memory T (T_{EM}) cells, known to mount rapid responses upon antigen re-exposure [29,42], were quantified in peripheral blood 20 days post-rechallenge to elucidate immune memory mechanisms. As shown in Fig. 3I-J, EPI/IMQ@Asphere-treated mice exhibited a 2.8-fold increase in $CD8^+$ T_{EM} cell frequency compared to the control group, demonstrating strong T cell memory responses by EPI/IMQ@Asphere for sustained antitumor immunity and recurrence prevention.

To explore the antitumor mechanism, the lymph nodes, spleen and tumor tissues were collected for immune profiling on day 12 post-administration (Fig. 4A). Flow cytometry analysis revealed that EPI/IMQ@Asphere induced higher proportion of mature DCs in lymph nodes than monotherapeutic EPI@Asphere and IMQ@Asphere (Fig. 4B). Mature DCs play a pivotal role in antigen presentation and T cell activation, a critical process for priming antitumor immunity as highlighted in prior studies [43]. Strikingly, EPI/IMQ@Asphere treatment induced a 7.0-fold increase in tumor-infiltrating cytotoxic $CD8^+$ T cells versus PBS group, substantially outperforming both EPI@Asphere (2.5-fold) and IMQ@Asphere (4.4-fold) monotherapies (Fig. 4C). Moreover, the expression levels of exhaustion markers (PD-1, TIM-3, LAG-3) on the tumor-infiltrating $CD8^+$ T cells in EPI/IMQ@Asphere cohort remained comparable to those in PBS group (Fig. S13), indicating that the infiltrating $CD8^+$ T cell remained functional and were not in an exhausted state. Additionally, increased M1 macrophage infiltration was observed in EPI/IMQ@Asphere-treated tumors, correlating with improved tumoricidal activity (Fig. 4D-E). Myeloid-derived suppressor cell (MDSCs) populations showed marked reduction following EPI/IMQ@Asphere treatment compared to PBS group (Fig. 4F and Fig. S14), indicating attenuated immunosuppressive tumor microenvironment. Meanwhile, the significant activation of DCs in the tumors as well as the marked reduction of MDSCs and Tregs in the spleens further verified the enhanced antitumor immune response of EPI/IMQ@Asphere treatment (Fig. 4G-I). Systemic immune activation was corroborated by elevated serum levels of proinflammatory cytokines including TNF-α, IL-6, and interferon-γ (IFN-γ) (Fig. 4J-L), consistent with established immune activation markers [19,44]. T cell depletion experiments demonstrated that the administration of anti-CD8 antibody substantially compromised the antitumor efficacy of EPI/IMQ@Asphere (Fig. S15), corroborating the critical role of adaptive antitumor immunity. These multifaceted immunomodulatory effects collectively underpin the superior tumor inhibition efficacy of EPI/IMQ@Asphere. Importantly, mice treated with EPI/IMQ@Asphere exhibited comparable counts of white blood cells, monocytes, and neutrophils to those in PBS group (Fig. S16). H&*E*-stained images revealed drug-loaded Asphere induced negligible damage in the vital organ tissues (Fig. S17). Moreover, no clinical signs (fever, lethargy, etc.) related to immune-related adverse events (irAE) were observed during the whole treatment period. These findings along with observed modest levels of pro-inflammatory cytokines indicate that EPI/IMQ@Asphere induce little immune-related adverse effects, likely attributable to the minimal drug deposition in the blood and major organs.

3.4. TACIE therapy with EPI/IMQ@Asphere for orthotopic liver tumors

Orthotopic VX2 liver cancer established by injecting VX2 tumor fragments into the liver parenchyma of rabbits [32,45], was employed to evaluate the TACIE therapy of EPI/IMQ@Asphere. Upon the tumor volume reaching around 800 mm^3 (day 0), the rabbits underwent transarterial embolization with EPI@CalliSpheres, EPI@Asphere, or EPI/IMQ@Asphere. In accordance with prior research findings [32,46,47], a low EPI dosage of 0.2 mg/kg was employed to attain optimal therapeutic efficacy while maintaining safety. As shown in Fig. 5A, EPI/IMQ@Asphere induced nearly complete vascular occlusion, signifying effective tumor-feeding artery blockade. CT and MRI imaging revealed rapid tumor progression in the PBS group, while all treatment groups displayed significant tumor growth suppression (Fig. 5B, and Fig. S18). Notably, EPI/IMQ@Asphere demonstrated the most pronounced therapeutic efficacy, showing marked tumor regression during treatment (Fig. 5C). H&E staining confirmed extensive necrosis across treatment groups, with EPI/IMQ@Asphere showing the largest necrotic areas (Fig. 5D). Immunofluorescence analysis revealed enhanced infiltration of $CD4^+$/$CD8^+$ T lymphocytes in all therapeutic groups, in which EPI/IMQ@Asphere generated over 4-fold increase of T cells compared to PBS group (Fig. 5 D—F), indicating robust activation of antitumor immunity. The tumor metastasis in the lung was monitored by CT imaging, the results showed that plenty of metastatic nodes in PBS group was significantly suppressed by all treatment groups, and EPI/IMQ@Asphere revealed superior metastasis control with few detectable lung nodules (Fig. 5I and Fig. S19). The efficient lung metastasis in EPI/IMQ@Asphere-treated mice was further verified by H&E staining (Fig. 5J-K), indicative of systemic antitumor effects against both primary tumors and distant metastases. The combination of TACE and immunotherapy has garnered considerable attention in recent research [6,48,49]. Clinical and preclinical evidence indicates that adjunctive intravenous administration of immune regulators such as checkpoint inhibitors during TACE markedly improves therapeutic outcomes. Despite improved antitumor activity, sustained tumor regression remains inconsistent, underscoring the need for refined therapeutic strategies to optimize outcomes.

The in vivo safety of embolic microspheres was assessed using H&E

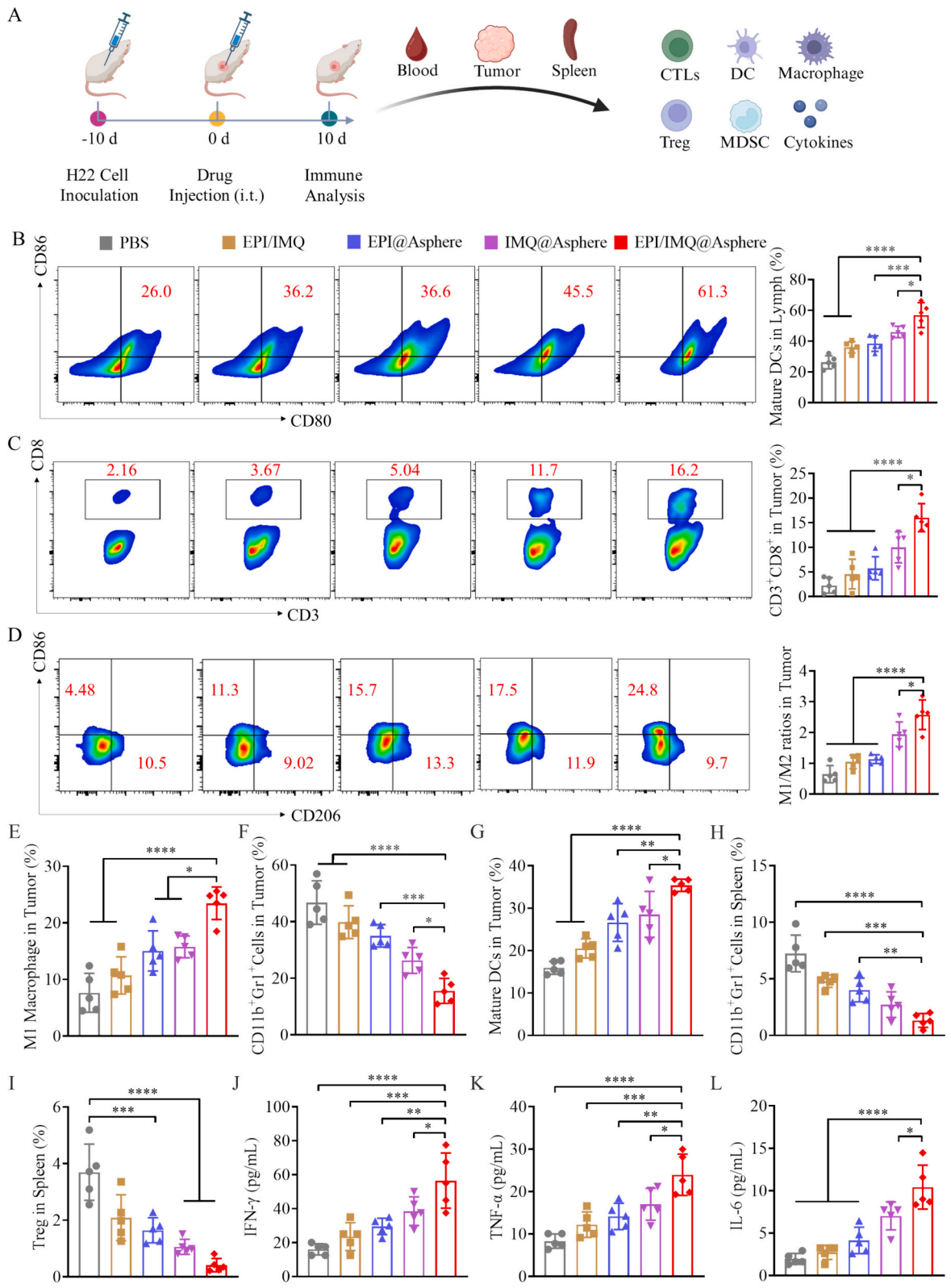

Fig. 4. In vivo immune activation in subcutaneous H22 tumor model. (A) Schematic diagram of the chemoimmunotherapy process, $n = 5$. (B) Representative flow cytometry graphs and quantification of Mature DCs cells in lymph. (C) Representative flow cytometry graphs and quantification of $CD3^+CD8^+$ T cells in tumors. (D) Representative flow cytometry graphs and quantification of the ratio of M1 to M2 macrophages in tumors. (E) Proportions of M1 macrophages ($CD11b^+CD86^+$) in tumors. (F-G) Proportions of $CD11b^+Gr1^+$ MDSCs cells (F) and mature DCs cells (G) in tumors. (H—I) Proportions of $CD11b^+Gr1^+$ MDSCs cells (H), $CD3^+CD4^+CD25^+Foxp3^+$ Treg cells (I) in spleens. (J-L) Expression levels of proinflammatory factors including IFN-γ (J), TNF-α (K), and IL-6 (L) in the serum analyzed by ELISA. Data are presented as the mean ± SD. Statistical significance was analyzed by one-way ANOVA using Tukey's posttest. p value: $^*p < 0.05$, $^{**}p < 0.01$, $^{***}p < 0.001$, $^{****}p < 0.0001$.

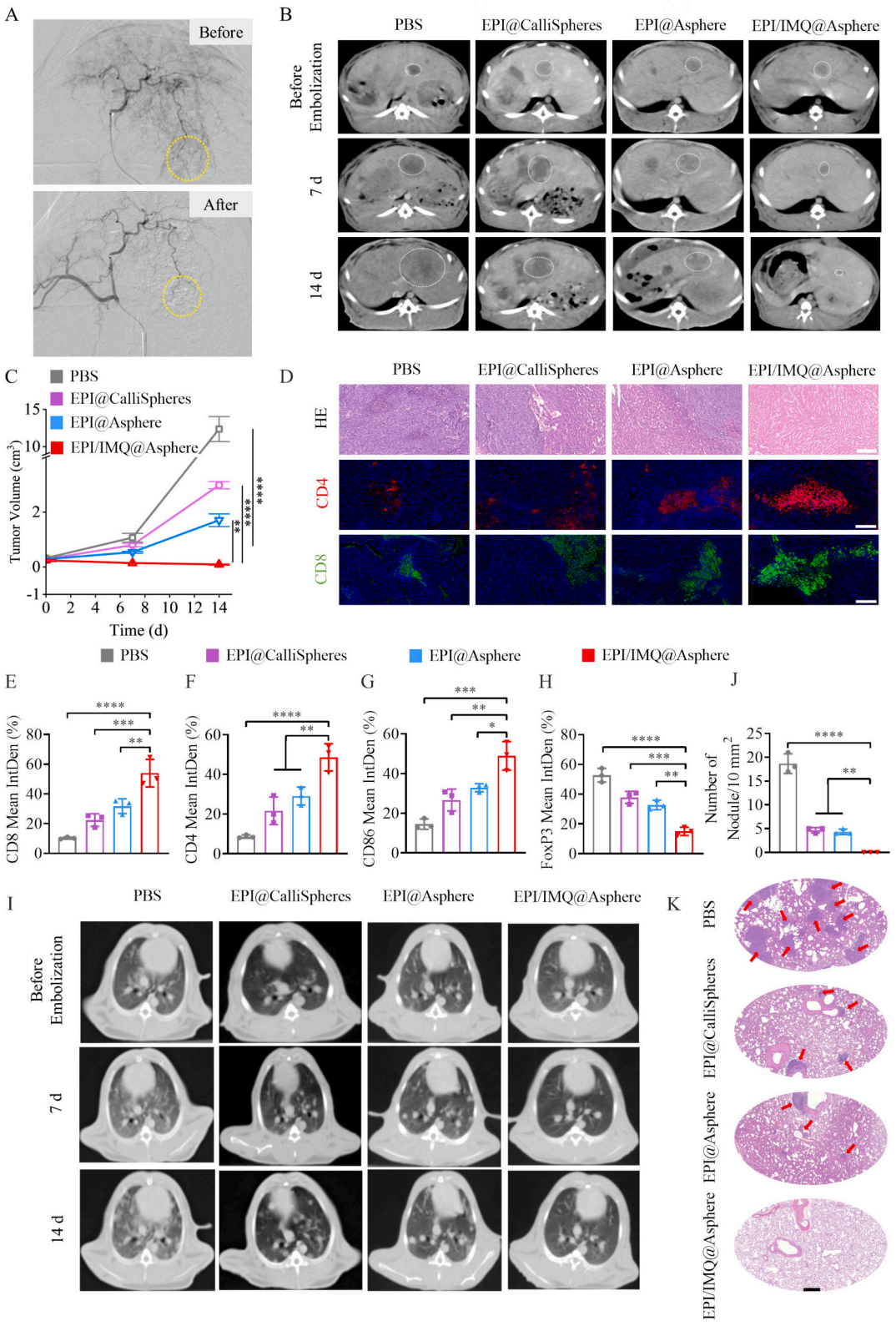

Fig. 5. TACIE therapy in orthotopic VX2 liver tumor-bearing rabbits. (A) Arterial angiography of tumors before and after TACIE using EPI/IMQ@Asphere. (B) Representative CT images of tumors on days 0, 7 and 14. (C) Tumor growth curves. (D) Representative H&E staining and CD4/CD8 immunofluorescent staining. Scale bar, 200 μm. (E-H) Statistical analysis of the average fluorescence intensity for CD8 (E), CD4 (F), CD86 (G), and FoxP3 (H) immunofluorescence staining, respectively ($n = 3$ biological samples). (I) Representative CT images of lung tissue on days 0 and 14. (J) Quantitative analysis of lung metastases. (K) Representative H&E staining slices of lung tissue on day 14. Scale bar, 500 μm. Data are presented as the mean ± SD. Statistical significance was analyzed by one-way ANOVA using Tukey's posttest. p value: $^{*}p < 0.05$, $^{**}p < 0.01$, $^{***}p < 0.001$, $^{****}p < 0.0001$.

staining and biochemical analysis. Compared to the PBS group, no obvious organ toxicity and damage were found in all treatment groups (EPI@CalliSpheres, EPI@Asphere, and EPI/IMQ@Asphere) (Fig. S20). Quantitative biochemical monitoring exhibited transient elevation of hepatic enzymes (ALT and AST) across all embolic treatment groups on day 3 post-treatment, followed by normalization to baseline levels. The transient hepatic function response aligns with established clinical manifestation of transarterial embolization procedures, which characteristically induce limited and reversible hepatocellular stress without persistent functional impairment [50]. Moreover, the levels of creatinine (Cr) and blood urea nitrogen (BUN) remained comparable across all experimental groups (Fig. S21), suggesting preserved renal function following treatment. These results illustrate that EPI/IMQ@Asphere-mediated interventional embolization shows decent biosafety profiles with negligible impacts on vital organ functions.

4. Conclusions

In summary, we have demonstrated that EPI/IMQ@Asphere combing efficient tumor vascular blockade, chemotherapy, and immunotherapy (TACIE) achieves potent suppression on tumor growth and metastasis in liver tumors. EPI/IMQ@Asphere exhibites nearly complete drug loading, superb stability, and sustained release of EPI (> 4 weeks) and IMQ. With continuous ICD generation and TLR7 stimulation, EPI/IMQ@Asphere induces persisting and marked DC activation, macrophage polarization, and proinflammatory cytokine secretion. In a subcutaneous H22 murine liver tumor model, one single administration of EPI/IMQ@Asphere confers potent tumor suppression, with complete regression in 5 out of 7 mice and complete resistance to tumor rechallenge. In orthotopic VX2 tumor-bearing rabbits, TACIE using EPI/IMQ@Asphere not only occludes tumor arteries and kills tumor cells but also amplifies tumoral $CD8^+/CD4^+$ T cell infiltration, achieving significant shrinkage of primary liver tumor and effective prevention of pulmonary metastasis. Therefore, EPI/IMQ@Asphere provides a potent therapeutic strategy for TACIE of advanced liver cancers.

CRediT authorship contribution statement

Yan Wang: Writing – original draft, Investigation, Data curation, Conceptualization. **Jiakun Guo:** Writing – original draft, Investigation, Data curation. **Di Hu:** Data curation. **Hujing Tan:** Formal analysis. **Wanting Chen:** Investigation. **Chao Deng:** Writing – review & editing, Supervision, Project administration, Funding acquisition, Conceptualization. **Xiaoli Zhu:** Conceptualization. **Zhiyuan Zhong:** Writing – review & editing, Conceptualization.

Acknowledgments

This work was financially supported by the National Natural Science Foundation of China (52373299, 51973149) and the National Key Research and Development Program of China (2021YFB3800900).

Appendix A. Supplementary data

Supplementary data to this article can be found online at https://doi.org/10.1016/j.jconrel.2025.114576.

Data availability

Data will be made available on request.

References

[1] F. Bray, M. Laversanne, H. Sung, J. Ferlay, R.L. Siegel, I. Soerjomataram, A. Jemal, Global cancer statistics, GLOBOCAN estimates of incidence and mortality worldwide for 36 cancers in 185 countries, CA Cancer J. Clin. 74 (2024) (2022) 229–263.

[2] J.M. Llovet, R.K. Kelley, A. Villanueva, A.G. Singal, E. Pikarsky, S. Roayaie, R. Lencioni, K. Koike, J. Zucman-Rossi, R.S. Finn, Hepatocellular carcinoma, Nat. Rev. Dis. Primers 7 (2021) 6.

[3] H. Rumgay, J. Ferlay, C.D. Martel, D. Georges, A.S. Ibrahim, R. Zheng, W. Wei, V.E. P.P. Lemmens, I. Soerjomataram, Global, regional and national burden of primary liver cancer by subtype, Eur. J. Cancer 161 (2022) 108–118.

[4] A. Forner, M. Gilabert, J. Bruix, J.L. Raoul, Treatment of intermediate-stage hepatocellular carcinoma, Nat. Rev. Clin. Oncol. 11 (2014) 525–535.

[5] M. Reig, A. Forner, J. Rimola, J. Ferrer-Fàbrega, M. Burrel, Á. Garcia-Criado, R. K. Kelley, P.R. Galle, V. Mazzaferro, R. Salem, B. Sangro, A.G. Singal, A. Vogel, J. Fuster, C. Ayuso, J. Bruix, BCLC strategy for prognosis prediction and treatment recommendation: the 2022 update, J. Hepatol. 76 (2022) 681–693.

[6] H.D. Zhu, H.L. Li, M.S. Huang, W.Z. Yang, G.W. Yin, B.Y. Zhong, J.H. Sun, Z.C. Jin, J.J. Chen, N.J. Ge, W.B. Ding, W.H. Li, J.H. Huang, W. Mu, S.Z. Gu, J.P. Li, H. Zhao, S.W. Wen, Y.M. Lei, Y.S. Song, C.W. Yuan, W.D. Wang, M. Huang, W. Zhao, J. B. Wu, S. Wang, X. Zhu, J.J. Han, W.X. Ren, Z.M. Lu, W.G. Xing, Y. Fan, H.L. Lin, Z. S. Zhang, G.H. Xu, W.H. Hu, Q. Tu, H.Y. Su, C.S. Zheng, Y. Chen, X.Y. Zhao, Z. T. Fang, Q. Wang, J.W. Zhao, A.B. Xu, J. Xu, Q.H. Wu, H.Z. Niu, J. Wang, F. Dai, D. P. Feng, Q.D. Li, R.S. Shi, J.R. Li, G. Yang, H.B. Shi, J.S. Ji, Y.E. Liu, Z. Cai, P. Yang, Y. Zhao, X.L. Zhu, L.G. Lu, G.J. Teng, Transarterial chemoembolization with PD-(L) 1 inhibitors plus molecular targeted therapies for hepatocellular carcinoma (CHANCE001), Signal Transduct. Target. Ther. 8 (2023) 1–10.

[7] Y. Ma, Z. Li, Y. Luo, Y. Chen, L. Ma, X. Liu, J. Xiao, M. Huang, Y. Li, H. Jiang, M. Wang, X. Wang, J. Li, J. Kong, P. Shi, H. Yu, X. Jiang, Q. Guo, Biodegradable microembolics with nanografted polyanions enable high-efficiency drug loading and sustained deep-tumor drug penetration for locoregional chemoembolization treatment, ACS Nano 18 (2024) 18211–18229.

[8] S. Shaha, D. Rodrigues, S. Mitragotri, Locoregional drug delivery for cancer therapy: preclinical progress and clinical translation, J. Control. Release 367 (2024) 737–767.

[9] L. Xue, A.S. Thatte, D. Mai, R.M. Haley, N. Gong, X. Han, K. Wang, N.C. Sheppard, C.H. June, M.J. Mitchell, Responsive biomaterials: optimizing control of cancer immunotherapy, Nat. Rev. Mater. 9 (2024) 100–118.

[10] Y.N. Fan, L. Zhu, Y.X. Qing, S.Y. Ye, Q.N. Ye, X.Y. Huang, D.K. Zhao, T.Y. Tian, F. C. Li, G.R. Yan, X.Z. Yang, S. Shen, J. Wang, Engineering multi-specific nano-antibodies for cancer immunotherapy, Nat. Biomed. Eng. 10 (2025) 1–17.

[11] Y. Guo, J. Pan, J. Wang, H. Zhang, W. Yang, F. Chen, B. Yin, X. Cai, W. Tao, T. Lammers, Y. Lai, H. Yu, X. Hu, Z. Xu, Engineering of sono-activatable immunogels for immunometabolism disorder normalization therapy of breast cancer, J. Am. Chem. Soc. 147 (2025) 22412–22426.

[12] Y. Engelen, R. Demuynck, J. Ramon, K. Breckpot, S.C. De Smedt, G.P.R. Lajoinie, K. Braeckmans, D.V. Krysko, I. Lentacker, Immunogenic cell death as interplay between physical anticancer modalities and immunotherapy, J. Control. Release 384 (2025) 113721.

[13] R. Wang, H. Li, S. He, Y. Feng, C. Liu, K. Hao, D. Zhou, X. Chen, H. Tian, Spatiotemporal nano-regulator unleashes anti-tumor immunity by overcoming dendritic cell tolerance and T cell exhaustion in tumor-draining lymph nodes, Adv. Mater. 37 (2025) 2412141.

[14] Y.Z. Li, C. Li, J.C. Yan, Y. Liao, C.Y. Qin, L.Y. Wang, Y. Huang, C. Yang, J.W. Wang, X. Ding, Y.Y. Yang, P.Y. Yuan, Polymeric micellar nanoparticles for effective CRISPR/Cas9 genome editing in cancer, Biomaterials 309 (2024) 122573.

[15] C. Yang, H. Zhang, L. Zhang, A.X. Zhu, R. Bernards, W. Qin, C. Wang, Evolving therapeutic landscape of advanced hepatocellular carcinoma, Nat. Rev. Gastroenterol. Hepatol. 20 (2023) 203–222.

[16] Y. Xie, H. Wu, Y. He, L. Liu, I.B. Huang, L. Zhou, C.Y. Lin, R.W.H. Leung, J.J. Loh, T.K.-W. Lee, J. Ding, K. Man, S. Ma, M. Tong, Targeting AXL induces tumor-intrinsic immunogenic response in tyrosine kinase inhibitor-resistant liver cancer, Cell Death Dis. 15 (2024) 110.

[17] S.L. Chan, B.Y. Ryoo, F. Mo, L.L. Chan, J. Cheon, L. Li, K.H. Wong, N. Yim, H. Kim, C. Yoo, Multicentre phase II trial of cabozantinib in patients with hepatocellular carcinoma after immune checkpoint inhibitor treatment, J. Hepatol. 81 (2024) 258–264.

[18] M. Park, J. Lim, S. Lee, Y. Nah, Y. Kang, W.J. Kim, Nanoparticle-mediated explosive anti-PD-L1 factory built in tumor for advanced immunotherapy, Adv. Mater. 37 (2025) 2417735.

[19] J. Guo, H. Tan, W. Chen, Y. Wang, W. Lin, Z. Zhong, C. Deng, Oncolytic microgels with regulated antibody release augment tumor immunotherapy, J. Control. Release 385 (2025) 114003.

[20] Q. Shi, W. Zhang, Y. Zhou, S. Huang, J. Yu, M. Yang, Z. Zhang, J. Ma, J. Luo, S. Rao, D. Lu, S. Peng, Y. Cao, L. Liu, Z. Yan, Hypoxia-activated cascade nanovaccine for synergistic chemoembolization-immune therapy of hepatocellular carcinoma, Biomaterials 306 (2024) 122480.

[21] L. Zhang, D. Wang, L.Z. Zhang, W.H. Yang, C. Yu, J. Qin, L.Z. Feng, Z. Liu, G. J. Teng, Pickering emulsion with tumor vascular destruction and microenvironment modulation for transarterial embolization therapy, Biomaterials 316 (2025) 123018.

[22] Y. Hao, W. Zhu, J. Li, R. Lin, W. Huang, Q.U. Ain, K. Liu, N. Wei, D. Cheng, Y. Wu, W. Lv, Sustained release hypoxia-activated prodrug-loaded BSA nanoparticles enhance transarterial chemoembolization against hepatocellular carcinoma, J. Control. Release 372 (2024) 155–167.

[23] Z.Y. Liu, H.Y. Chu, W.D. Zhao, C.G. Yang, T.J. Liu, N. Shen, Z.H. Tang, Polymeric multivalent fc binding peptides-fabricated clinical compounding bispecific antibody potentiates dual immunotherapy targeting PD1 and CTLA-4, Adv. Sci. 12 (2025) 2408899.

[24] X. Xia, Y. Li, R. Huang, Y. Wang, W. Xiong, H. Zhou, M. Li, X. Lin, Y. Tang, B. Zhang, A lipiodol Pickering emulsion stabilized by iron-doped carbon

nanozymes for liver transarterial chemoembolization, Adv. Sci. 12 (2025) 2410873.
[25] Y. Peng, H. Liu, X. Liang, L. Cao, M. Teng, H. Chen, Z. Li, X. Peng, J. Mao, H. Cheng, G. Liu, Self-assembling chemodrug fiber-hydrogel for transarterial chemoembolization and radiotherapy-enhanced antitumor immunity, J. Control. Release 380 (2025) 1–16.
[26] M. Li, D. Zhao, J. Yan, X. Fu, F. Li, G. Liu, Y. Fan, Y. Liang, X. Zhang, A redox-triggered autophagy-induced nanoplatform with PD-L1 inhibition for enhancing combined chemo-immunotherapy, ACS Nano 18 (2024) 12870–12884.
[27] Z.L. Li, H. Cai, Z.Q. Li, L. Ren, X.L. Ma, H.Y. Zhu, Q.Y. Gong, H. Zhang, Z.W. Gu, K. Luo, A tumor cell membrane-coated self-amplified nanosystem as a nanovaccine to boost the therapeutic effect of anti-PD-L1 antibody, Bioact. Mater. 21 (2023) 299–312.
[28] J.Y. Li, H.A. Faruque, S.N. Li, M. Sima, D. Sborov, S. Hu-Lieskovan, T. Werner, Jindřich Kopeček, J.Y. Yang, PD-L1 targeted antibody-polymer-Epirubicin conjugate prolongs survival in a preclinical murine model of advanced ovarian cancer, J. Control. Release 382 (2025) 113682.
[29] P.H. Chao, V. Chan, J. Wu, L.J. Andrew, S.D. Li, Resiquimod-loaded cationic liposomes cure mice with peritoneal carcinomatosis and induce specific anti-tumor immunity, J. Control. Release 372 (2024) 362–371.
[30] S. Sun, Y. He, J. Xu, S. Leng, Y. Liu, H. Wan, L. Yan, Y. Xu, Enhancing cell pyroptosis with biomimetic nanoparticles for melanoma chemo-immunotherapy, J. Control. Release 367 (2024) 470–485.
[31] Y. Xing, R. Wu, Z. Tu, M. Meng, L. Xiang, H. Li, Z. Shi, G. Fang, Y. Feng, Z. Li, H. Tian, X. Chen, Precisely deliver toll-like receptor agonists using a dual-responsive nanovaccine for effective cancer immunotherapy, Biomaterials 324 (2026) 123527.
[32] J. Guo, J. Huang, Z. Huang, D. Hu, H. Tan, Y. Wang, C. Deng, X. Zhu, Z. Zhong, Tumor vessel-adaptable adhesive and absorbable microspheres for sustainable transarterial chemoembolization therapy, Nat. Commun. 16 (2025) 6239.
[33] J. Dong, Y. Lang, J. He, J. Cui, X. Liu, H. Yuan, L. Li, M. Zhou, S. Wang, Phycocyanin-based multifunctional microspheres for treatment of infected radiation-induced skin injury, Biomaterials 317 (2025) 123061.
[34] Y. Li, S. Han, Y. Zhao, J. Yan, K. Luo, F. Li, B. He, Y. Sun, F. Li, Y. Liang, A redox-triggered polymeric nanoparticle for disrupting redox homeostasis and enhanced ferroptosis, Small 21 (2025) 2404299.
[35] X.D. Wen, X. Xiong, G. Yang, W.J. Xiao, J. Hou, T. Pan, Y.H. Hu, S.B. Zhou, A macrophage membrane-coated mesoporous silica nanoplatform inhibiting adenosine A2AR via in situ oxygen supply for immunotherapy, J. Control. Release 353 (2023) 535–548.
[36] M.Y. He, M.Y. Zhang, T. Xu, S.J. Xue, D.Z. Li, Y.N. Zhao, F. Zhi, D.W. Ding, Enhancing photodynamic immunotherapy by reprograming the immunosuppressive tumor microenvironment with hypoxia relief, J. Control. Release 368 (2024) 233–250.
[37] X.Y. Wang, X.F. Zhong, Z.Q. Xie, Y.H. Zhao, H.R. Wang, Z.R. Zhang, T. Gong, G. S. Du, X. Sun, A trinity strategy: mesoporous platinum nanoparticles serve as a photoenhanced nanoplatform for tumor immunotherapy, Chem. Eng. J. 495 (2024) 153365.
[38] Y. Guo, Y. Li, M. Zhang, R. Ma, Y. Wang, X. Weng, J. Zhang, Z. Zhang, X. Chen, W. Yang, Polymeric nanocarrier via metabolism regulation mediates immunogenic cell death with spatiotemporal orchestration for cancer immunotherapy, Nat. Commun. 15 (2024) 8586.
[39] X. Wu, J. Zhang, Z. Deng, X. Sun, Y. Zhang, C. Zhang, J. Wang, X. Yu, G. Yang, Bacteria-based biohybrids for remodeling adenosine-mediated immunosuppression to boost radiotherapy-triggered antitumor immune response, Biomaterials 316 (2025) 123000.
[40] Y. Zhang, Z. Yan, S. Geng, Y. Wang, J. Ren, Y. Jiang, L. Yang, W. Dai, H. Zhang, X. Wang, N. Zheng, Q. Zhang, B. He, A nanoscale innate immune multiplier amplifies immunogenic cell death triggered by oxaliplatin via enhancing systemic and trained immunity, Nano Today 65 (2025) 102835.
[41] T. Wang, J. Ding, S. Liang, Z. Lin, J. Yang, Z. Zhang, Z. Zou, G. Li, X. Chen, C. He, An adhesive immune-stimulating multifunctional hydrogel for potent tumor chemoimmunotherapy and postoperative wound healing promotion, Adv. Funct. Mater. 34 (2023) 2312360.
[42] S.E. Ackerman, C.I. Pearson, J.D. Gregorio, J.C. Gonzalez, J.A. Kenkel, F. J. Hartmann, A. Luo, P.Y. Ho, H. LeBlanc, L.K. Blum, S.C. Kimmey, A. Luo, M. L. Nguyen, J.C. Paik, L.Y. Sheu, B. Ackerman, A. Lee, H. Li, J. Melrose, R.P. Laura, V.C. Ramani, K.A. Henning, D.Y. Jackson, B.S. Safina, G. Yonehiro, B.H. Devens, Y. Carmi, S.J. Chapin, S.C. Bendall, M. Kowanetz, D. Dornan, E.G. Engleman, M. N. Alonso, Immune-stimulating antibody conjugates elicit robust myeloid activation and durable antitumor immunity, Nat. Can. 2 (2021) 18–33.
[43] S. Lv, K. Song, A. Yen, D.J. Peeler, D.C. Nguyen, A. Olshefsky, M. Sylvestre, S. Srinivasan, P.S. Stayton, S.H. Pun, Well-defined mannosylated polymer for peptide vaccine delivery with enhanced antitumor immunity, Adv. Healthc. Mater. 11 (2022) 2101651.
[44] H. Tan, J. Guo, Y. Wang, W. Chen, Z. Zhong, C. Deng, Long-acting in situ cancer vaccines by oncolytic sting-activating microgels, Small 22 (2025) e03561.
[45] Y. Wang, X. He, C. Zhou, Y. Bai, T. Li, J. Liu, S. Ju, C. Wang, G. Xiang, B. Xiong, Nanoscale CaO_2 materials for synergistic transarterial chemoembolization in a VX2 orthotopic rabbit liver cancer model, Acta Biomater. 154 (2022) 536–548.
[46] D. Kim, J.H. Lee, H. Moon, M. Seo, H. Han, H. Yoo, H. Seo, J. Lee, S. Hong, P. Kim, H.J. Lee, J.W. Chung, H. Kim, Development and evaluation of an ultrasound-triggered microbubble combined transarterial chemoembolization (TACE) formulation on rabbit VX2 liver cancer model, Theranostics 11 (2021) 79–92.
[47] F. Gong, L. Zheng, J. Xu, Y. Wu, Q. Jin, J. Lu, Z. Pei, Z. Zhao, M. Chen, J. Tu, S. Fang, W. Chen, K. Wei, N. Yang, C. Gong, F. Wu, Y. Zhang, C. Ni, L. Cheng, Z. Liu, J. Ji, Magnesium microspheres for enhanced transarterial chemoembolization therapy of hepatocellular carcinoma: from animal models to a pilot clinical study, Sci. Adv. 11 (2025) eadv0885.
[48] Immune checkpoint inhibitors and anti-vascular endothelial growth factor antibody/tyrosine kinase inhibitors with or without transarterial chemoembolization as first-line treatment for advanced hepatocellular carcinoma (CHANCE2201): a target trial emulation study, EClinicalMedicine 72 (2024) 102622.
[49] J. Xu, Z. Pei, Y. Wang, N. Jiang, Y. Gong, F. Gong, C. Ni, L. Cheng, Bioactive microspheres to enhance sonodynamic-embolization-metalloimmune therapy for orthotopic liver cancer, Biomaterials 317 (2025) 123063.
[50] M. Chen, Q. Lu, F. Gong, Y. Yang, Z. Pei, X. Huang, G. Shu, L. Shen, P. Yan, X. Guo, Z. Liu, L. Cheng, J. Ji, A gas nanobomb to promote drug penetration and amplify tace therapy for orthotopic liver tumor, Adv. Mater. 38 (2025) 2505770.